Hindawi Publishing Corporation
Advances in Materials Science and Engineering
Volume 2015, Article ID 649046, 10 pages
http://dx.doi.org/10.1155/2015/649046

Research Article

Multiobject Reliability Analysis of Turbine Blisk with Multidiscipline under Multiphysical Field Interaction

Chun-Yi Zhang,[1] Cheng Lu,[1] Cheng-Wei Fei,[2,3] Ling-Jun Liu,[1] Yat-Sze Choy,[2] and Xiang-Guo Su[1]

[1]*School of Mechanical and Power Engineering, Harbin University of Science and Technology, Harbin 150080, China*
[2]*Department of Mechanical Engineering, The Hong Kong Polytechnic University, Kowloon, Hong Kong*
[3]*School of Energy and Power Engineering, Beihang University, Beijing 100191, China*

Correspondence should be addressed to Cheng-Wei Fei; feicw544@163.com

Received 6 May 2015; Revised 30 June 2015; Accepted 8 July 2015

Academic Editor: Anna Richelli

To study accurately the influence of the deformation, stress, and strain of turbine blisk on the performance of aeroengine, the comprehensive reliability analysis of turbine blisk with multiple disciplines and multiple objects was performed based on multiple response surface method (MRSM) and fluid-thermal-solid coupling technique. Firstly, the basic thought of MRSM was introduced. And then the mathematical model of MRSM was established with quadratic polynomial. Finally, the multiple reliability analyses of deformation, stress, and strain of turbine blisk were completed under multiphysical field coupling by the MRSM, and the comprehensive performance of turbine blisk was evaluated. From the reliability analysis, it is demonstrated that the reliability degrees of the deformation, stress, and strain for turbine blisk are 0.9942, 0.9935, 0.9954, and 0.9919, respectively, when the allowable deformation, stress, and strain are 3.7×10^{-3} m, 1.07×10^{9} Pa, and 1.12×10^{-2} m/m, respectively; besides, the comprehensive reliability degree of turbine blisk is 0.9919, which basically satisfies the engineering requirement of aeroengine. The efforts of this paper provide a promising approach method for multidiscipline multiobject reliability analysis.

1. Introduction

An aeroengine as the power system of aircraft seriously influences the performance and reliability of air vehicle [1]. Bladed disk as one pivotal part of aeroengine is the important fault source of aeroengine for suffering from high temperature, high pressure, and high rotation speed during operation [2]. Of the faults of aeroengine, the rate of blisk fault is 25%. The performances of aeroengine safety, reliability, and robustness are to decline sharply once blisk fault occurs [3]. Therefore, it is of great significance for improving the whole performance and reliability of aeroengine to investigate the reliability of blisk.

Recently, some efforts spring up on the improvement of aeroengine. Qi et al. studied the time history variation of the blade-tip clearance of aeroengine high turbine by finite element method under considering the effects of temperature, pressure, and rotation speed [4]. Pillidis and Maccallum, focused on the change rule of aeroengine high-pressure blade-tip radial running clearance through calculating the radial deformations of turbine disk, blade, and casing by adopting thermal-solid coupling method under the influences of heat load and centrifugal force load [5]. Wang et al. analyzed the stress of contact region on the blade and disk of aeroengine based on finite element method [6]. Meguid et al. discussed the effect of impact force by simulating the impact of bird against the blade of aeroengine using finite element method [7]. The above investigations only focus on the deterministic analysis without considering the randomness of influencing parameter on aeroengine blisk, so that it is very difficult to gain reasonable results for blisk design and analysis.

To address this issue, one viable alternative to deterministic analysis is probabilistic analysis, which does consider the randomness of factors to describe the blisk deformation of aeroengine with acceptable accuracy. The probabilistic

analysis method has been widely applied in many fields. For instance, Lü and Low conducted the probabilistic analysis of underground rock excavations [8]; Kartal et al. implemented the probabilistic nonlinear analysis of CFR dams [9]; Fitzpatrick et al. applied probabilistic analysis method to multivariate sensitivity evaluation patellofemoral mechanics [10]; Zona et al. studied design assessment of continuous steel concrete composite girders with probabilistic analysis [11]. Meanwhile, some works were also done in the probabilistic analysis of typical aeroengine components. Hu et al. researched the probabilistic design for turbine disk at high temperature [12]; Nakamura and Fujii analyzed the transient heat of an atmospheric reentry vehicle structure using probabilistic method [13]; Fei et al. finished the probabilistic analyses of turbine disk [14] and casing [15, 16]. Additionally, some approaches of probabilistic analysis have been developed such as Monte Carlo method (MCM) [13], response surface method (RSM) [17, 18], extremum response surface method [14, 15], and support vector machine [16, 19], for the probabilistic analyses and reliability analyses of typical aeroengine components and the blade-tip radial running clearance of aeroengine high-pressure turbine. The efforts only keep a watchful eye on the reliability analysis of single object which needs to build one model and do not consider the influences of all factors. In fact, although the computational precision and efficiency were greatly improved by the above method, blisk reliability is determined by many failure models and multiple disciplines. Although multiple response surface model (MRSM) was developed for the reliability analysis of aeroengine blade-tip clearance by establishing many response surface models for different disciplines [18], two deficiencies yet exist: (1) only consider the influence of centrifugal load and heat load without the effect due to fluid; (2) only finish the reliability analysis of single object by single response surface model without considering multiple output response (multiobject) by multiple response surface models.

To solve the above issues, accompanied with the heuristic idea of MRSM [18], the comprehensive reliability analysis of aeroengine turbine blisk with multifailure models (multiobject) was completed by considering multidiscipline of heat, fluid, and structure.

In what follows, Section 2 introduces the basic thought of MRSM and establishes its mathematical model based on quadratic polynomial. In Section 3, the fluid-thermal-structural analysis of turbine blisk is completed by considering various parameters from different disciplines. Section 4 focuses on the comprehensive reliability evaluation of turbine blisk from the reliability analyses of deformation, stress, and strain of blisk under the effect of fluid-thermal-solid interaction. Section 5 summarizes the conclusions of this work.

2. Multiple Response Surface Method (MRSM)

2.1. Basic Principle. For structural reliability analysis with multiple disciplines and multiple objects, MRSM is structured and applied based on response surface method. The basic thought of MRSM is summarized as follows:

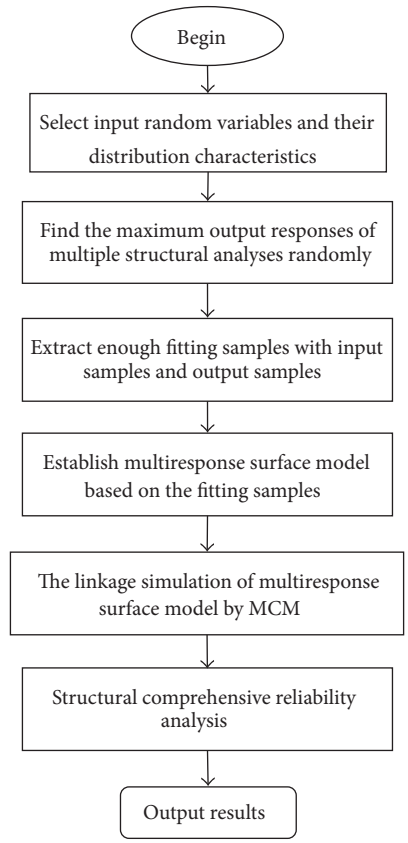

Figure 1: Flow chart of structural reliability analysis based on MRSM.

(1) Select input random variables reasonably to complete the deterministic analyses of multiple objects for complex structure.

(2) Find the maximum values of multiobject analytical results as output responses to complete multiobject reliability analysis.

(3) Structure the multiple response surface models by extracting the samples of input variables and calculating the output response of each object based on simulation methods like MCM [13].

(4) The reliability analysis of complex structure with multidiscipline and multiobject is completed by simulating the multiple response surface models by using MCM.

The flow chart of structural reliability analysis based on MRSM is shown in Figure 1.

2.2. Mathematical Model of MRSM. Response surface method (RSM) is used to fit a simple response surface by a series of deterministic analyses replacing the real limit-state function [15]. When y and $\mathbf{X}$ express the output response and the vector of input random variables, respectively,

the quadratic polynomial response surface function is structured as follows:

$$y(\mathbf{X}) = A + \mathbf{B}\mathbf{X} + \mathbf{X}^{\mathrm{T}}\mathbf{C}\mathbf{X} \tag{1}$$

in which A, $\mathbf{B}$, and $\mathbf{C}$ are the coefficient of constant, the vector of linear term coefficients, and the matrix of quadratic term coefficients, respectively. $\mathbf{B}$, $\mathbf{C}$, and $\mathbf{X}$ are denoted by

$$\mathbf{B} = \begin{bmatrix} b_1 & b_2 & \cdots & b_k \end{bmatrix},$$

$$\mathbf{C} = \begin{bmatrix} c_{11} & & & & \\ & c_{22} & & & \\ & & c_{33} & & \\ & & & \ddots & \\ & & & & c_{kk} \end{bmatrix}, \tag{2}$$

$$\mathbf{X} = \begin{bmatrix} x_1 & x_2 & \cdots & x_k \end{bmatrix}^{\mathrm{T}},$$

where k is the number of input random variables.

In this paper, the mathematical model of MRSM was established on the foundation of quadratic polynomial response surface function. Assuming that the reliability analysis of a complex structure involves m ($m \in Z$) output objects, the input random variable vector of the ith output object is $\mathbf{X}^{(i)}$, and the corresponding output variable is denoted by $y^{(i)}$, the relationship of $\mathbf{X}^{(i)}$ and $y^{(i)}$ is

$$y^{(i)} = f\left(\mathbf{X}^{(i)}\right) \quad (i = 1, 2, \ldots, m) \tag{3}$$

in which $f(\cdot)$ is the function of input random variables.

In the light of quadratic polynomial response surface function, (3) is rewritten as

$$y^{(i)}\left(\mathbf{X}^{(i)}\right) = A^{(i)} + \mathbf{B}^{(i)}\mathbf{X}^{(i)} + \left(\mathbf{X}^{(i)}\right)^{\mathrm{T}}\mathbf{C}^{(i)}\mathbf{X}^{(i)}, \tag{4}$$

where $A^{(i)}$ is the constant coefficient of the ith output object, $\mathbf{B}^{(i)}$ the coefficient vector of linear term of the ith output object, and $\mathbf{C}^{(i)}$ the coefficient matrix of quadratic term.

Equation (4) is also reshaped as

$$y^{(i)} = a^{(i)} + \sum_{j=1}^{k} b_j^{(i)} x_j^{(i)} + \sum_{j=1}^{k} c_j^{(i)} \left(x_j^{(i)}\right)^2 \quad (p = 1, 2, \ldots, k) \tag{5}$$

in which $x_j^{(i)}$ denotes the jth component of the input variable x in the ith output response (object) and $a^{(i)}$, $b_j^{(i)}$, and $c_j^{(i)}$ denote the undetermined coefficients of constant term, linear term, and quadratic term, respectively. The number of undetermined coefficients is $m(2k + 1)$. The undetermined coefficients are gained based on least square method when the number of samples is enough, because the vector $\mathbf{D}^{(i)}$ is formed by

$$\mathbf{D}^{(i)} = \left[A^{(i)} \;\; b_1^{(i)} \;\; b_2^{(i)} \;\; \cdots \;\; b_k^{(i)} \;\; c_{11}^{(i)} \;\; c_{22}^{(i)} \;\; \cdots \;\; c_{kk}^{(i)}\right]. \tag{6}$$

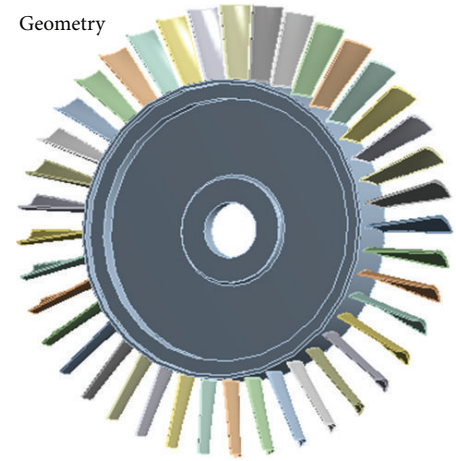

Figure 2: Structure model of blisk.

From (4), $\mathbf{D}^{(i)}$ may be deduced as

$$\mathbf{D}^{(i)} = \left[\left(\mathbf{X}^{(i)}\right)^{\mathrm{T}}\mathbf{X}^{(i)}\right]^{-1}\left(\mathbf{X}^{(i)}\right)^{\mathrm{T}} y^{(i)}. \tag{7}$$

From (6), we can gain the undetermined coefficients of (5) and further the mathematical model of MRSM is

$$\begin{aligned} y^{(1)} &= a^{(1)} + \sum_{j=1}^{k} b_j^{(1)} x_j^{(1)} + \sum_{j=1}^{k} C_j^{(1)} \left(x_j^{(1)}\right)^2 \\ y^{(2)} &= a^{(2)} + \sum_{j=1}^{k} b_j^{(2)} x_j^{(2)} + \sum_{p=1}^{k} C_j^{(2)} \left(x_j^{(2)}\right)^2 \\ &\vdots \\ y^{(m)} &= a^{(m)} + \sum_{j=1}^{k} B_j^{(m)} x_j^{(m)} + \sum_{j=1}^{k} C_j^{(m)} \left(x_j^{(m)}\right)^2. \end{aligned} \tag{8}$$

3. Fluid-Thermal-Solid Coupling Analysis of Turbine Blisk

The working condition of aeroengine is so harsh that the blisk of turbine suffers from the high-temperature gas and large centrifugal force. To simulate the real work condition of turbine blisk, the fluid-thermal-solid coupling analysis was executed based on the discrete coupling analysis method [20, 21]. Therein, the structure of turbine blisk is shown in Figure 2 and TC4 alloy was selected as the material of turbine blisk. In this deterministic analysis, the inlet speed is 160 m/s, the inlet pressure is 600 000 Pa, gas temperature is 1150 K, and the rotation speed of blisk is 1168 rad/s [17–19]. The inlet flow velocity v of air, inlet pressure p, material density ρ, temperature t, and rotation speed w were selected as random variables obeying normal distributions with mutual independence.

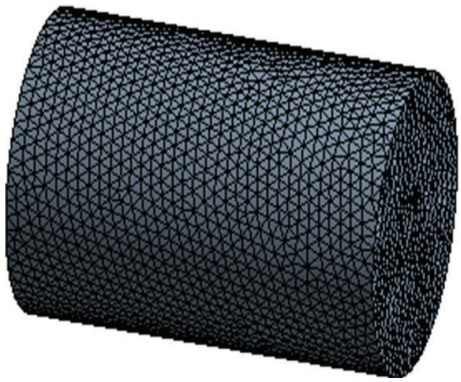

Figure 3: Flow field grid of blisk.

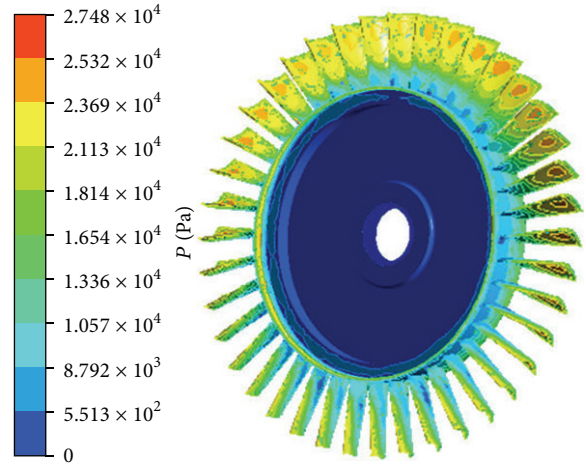

Figure 4: Static pressure distribution of blisk surface.

3.1. Fluid Analysis of Turbine Blisk. In fluid analysis, the standard k-ε turbulence model [22, 23] without gravity effect was selected as follows:

$$\begin{aligned}
&\frac{\partial}{\partial t}(\rho k) + \frac{\partial}{\partial x_i}(\rho k u_i) \\
&\quad = \frac{\partial}{\partial x_j}\left[\left(\mu + \frac{\mu_t}{\sigma_k}\right)\frac{\partial k}{\partial x_j}\right] + G_k + G_b - \rho\varepsilon - Y_M \\
&\qquad + S_k, \\
&\frac{\partial}{\partial t}(\rho\varepsilon) + \frac{\partial}{\partial x_i}(\rho\varepsilon u_i) \\
&\quad = \frac{\partial}{\partial x_j}\left[\left(\mu + \frac{\mu_t}{\sigma_\varepsilon}\right)\frac{\partial \varepsilon}{x_j}\right] + C_{1\varepsilon}\frac{\varepsilon}{k}(G_k + C_{3\varepsilon}G_b) \\
&\qquad - C_{2\varepsilon}\rho\frac{\varepsilon^2}{k} + S_\varepsilon, \\
&\mu_t = \rho C_\mu \frac{k^2}{\varepsilon},
\end{aligned} \tag{9}$$

where k is the turbulence energy; ε the specific dissipation rate; μ_t the eddy viscosity; G_k the turbulence energy generated from the mean velocity gradient; G_b the turbulence energy generated from flotage; and Y_M the effect of the fluctuating expansion of compressible speed turbulence on the total dissipation rate. The coefficients C_μ, σ_k, σ_ε, $C_{1\varepsilon}$, $C_{2\varepsilon}$, and $C_{3\varepsilon}$ were the constants of 0.09, 1, $\sigma_\varepsilon = 1.3$, $C_{1\varepsilon} = 1.44$, and $C_{2\varepsilon} = 1.92$, respectively, and the G_b and Y_M were not considered in fluid analysis. The flow field model of turbine blisk is built with the diameter 1.2 m and the length 2 m. The finite element model of flow field was established as shown in Figure 3 with the number of elements being 589 428 and the number of nodes being 842 703. In line with the boundary condition of blisk flow field, the numerical simulation analysis of flow field was completed based on the finite element volume method and k-ε standard turbulence model. From the analysis, the static pressure distribution of turbine blisk is revealed in Figure 4.

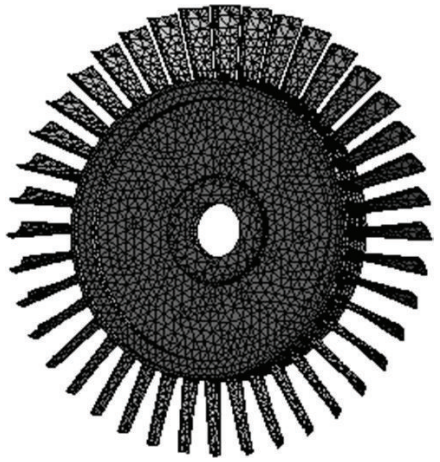

Figure 5: Grid of blisk.

3.2. Thermal Analysis of Turbine Blisk. The thermal analysis of turbine blisk was finished based on the following energy conservation equation [23]:

$$\begin{aligned}
&\frac{\partial}{\partial t}\left(\rho C_p T_0\right) + \frac{\partial}{\partial x}\left(\rho v_x C_p T_0\right) + \frac{\partial}{\partial y}\left(\rho v_y C_P T_0\right) \\
&\qquad + \frac{\partial}{\partial z}\left(\rho v_z C_p T_0\right) \\
&\quad = \frac{\partial}{\partial x}\left(K\frac{\partial T_0}{\partial x}\right) + \frac{\partial}{\partial y}\left(K\frac{\partial T_0}{\partial y}\right) + \frac{\partial}{\partial z}\left(K\frac{\partial T_0}{\partial z}\right) \\
&\qquad + W_v + E_k + Q_v + \Phi + \frac{\partial P}{\partial t}
\end{aligned} \tag{10}$$

in which C_p is the specific heat, T_0 the total temperature, K the heat conductivity coefficient, W_v the viscous dissipation, E_k the kinetic energy, Q_v the volume heat source, and Φ the item of viscous heat.

The finite element model of turbine blisk was built as shown in Figure 5, which includes the number of elements, 34 875, and the number of nodes, 68 678. The heat loads

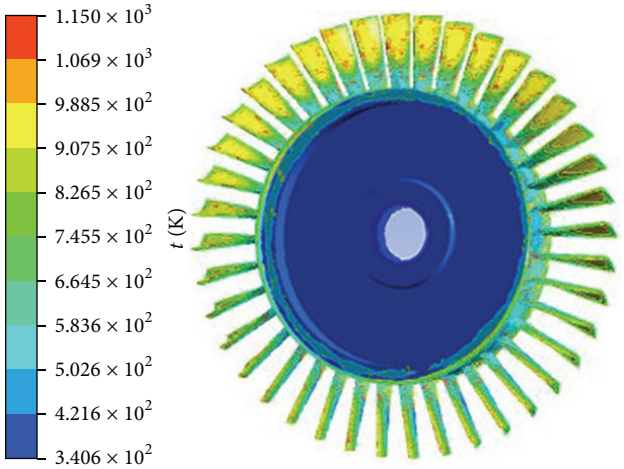

Figure 6: Temperature distribution of blisk surface.

from high-temperature gas were exerted on the blisk of turbine, where the temperature distribution of turbine blisk is demonstrated in Figure 6.

3.3. Structural Analysis of Turbine Blisk. Tetrahedron was selected as the element of blisk's finite element model. The structural analysis of turbine blisk was performed by transforming the analytical results of fluid analysis and thermal analysis into the surface of turbine blisk based on finite element method. In order to more accurately express the results of structure analysis, the shape function of tetrahedron elements (in (11)) and the displacement equations (in (12)) [24] are applied to solve the node deformation of turbine blisk. The concentrated force and moment of joints are equivalent to the distribution force based on the results of nodes deformation and the relationship between displacement and stress (in (13)). Besides, the strain results of turbine blisk are gained by using (14).

The shape function of tetrahedron elements is

$$N_i = \frac{1}{6V}\left(a_i + b_i x + c_i y + d_i z\right) \quad (i = 1, 2, 3, 4); \tag{11}$$

here V is the volume of tetrahedron and a_i, b_i, c_i, and d_i are the related coefficients of node geometry.

The displacement equations of element node on three directions are

$$\begin{aligned} u(x, y, z) &= a_0 + a_1 x + a_2 y + a_3 z, \\ v(x, y, z) &= b_0 + b_1 x + b_2 y + b_3 z, \\ w(x, y, z) &= c_0 + c_1 x + c_2 y + c_3 z. \end{aligned} \tag{12}$$

The relationship between displacement and stress on the element of turbine blisk is denoted by

$$\begin{aligned} \sigma_x &= \frac{\partial u}{\partial x}; \\ \sigma_y &= \frac{\partial v}{\partial y}; \\ \sigma_z &= \frac{\partial w}{\partial z}, \\ \gamma_{xy} &= \frac{\partial u}{\partial y} + \frac{\partial v}{\partial x}; \\ \gamma_{yz} &= \frac{\partial v}{\partial z} + \frac{\partial w}{\partial y}; \\ \gamma_{zx} &= \frac{\partial u}{\partial z} + \frac{\partial w}{\partial x}. \end{aligned} \tag{13}$$

Table 1: Input random variables of MRSM reliability analysis.

Input random variables	Distribution	Mean	Standard deviation
Inlet speed, v/(m/s)	Normal	160	3.2
Inlet pressure, p/Pa	Normal	600 000	18 000
Temperature, t/K	Normal	1150	15.56
Material density, ρ/(kg/m^3)	Normal	4 620	92.4
Rotation speed, w/(rad/s)	Normal	1168	23.36

The relationship between stress and strain on the element of turbine blisk is expressed by

$$\{\boldsymbol{\sigma}\} = [\mathbf{D}]\left\{\boldsymbol{\varepsilon}^{\mathrm{el}}\right\}, \tag{14}$$

where σ_x, σ_y, and σ_z and γ_{xy}, γ_{yz}, and γ_{zx} are the normal stresses and shear stresses on x, y, and z directions, respectively; $\{\boldsymbol{\sigma}\} = [\sigma_x, \sigma_y, \sigma_z, \gamma_{xy}, \gamma_{yz}, \gamma_{zx}]^{\mathrm{T}}$ are the components of stress; $[\mathbf{D}]$ is the elastic matrix (or elastic stiffness matrix or the stress and strain matrix); $\{\boldsymbol{\varepsilon}^{\mathrm{el}}\}$ is the vector of elastic strain.

Under the effect of fluid pressure, heat stress, and centrifugal force, the deformation, stress, and strain of turbine blisk were analyzed. From this analysis, the nephograms of deformation, stress, and strain are listed in Figure 7. In Figure 7, u, σ, and ε indicate the deformation, stress, and strain of turbine blisk (similarly hereinafter). The changing curves of deformation, stress, and strain are shown in Figure 8. Figures 7 and 8 reveal that the maximum deformation locates on the blade-tip of turbine blisk, while the maximum stress and strain locate on root of turbine blisk.

As shown in Figures 7 and 8, the highest temperature locates on the top of blisk; meanwhile, the temperature gradually reduces from the top of blisk to the root of blisk. However, the maximum stress and strain are on the root of blisk, and the stress and strain decrease from the root of blisk to the top of blisk in which the variations of the stress and strain of turbine blisk hold close relationship with the geometrical shape of turbine blisk. The above conclusions are consistent with practical engineering.

4. Reliability Analysis of Turbine Blisk

In the light of the results of fluid-thermal-solid coupling analysis, the points corresponding to the maximum values of blisk's deformation, stress, and strain are regarded as the computational point of reliability analysis of turbine blisk. In accordance with the input random variables in Table 1

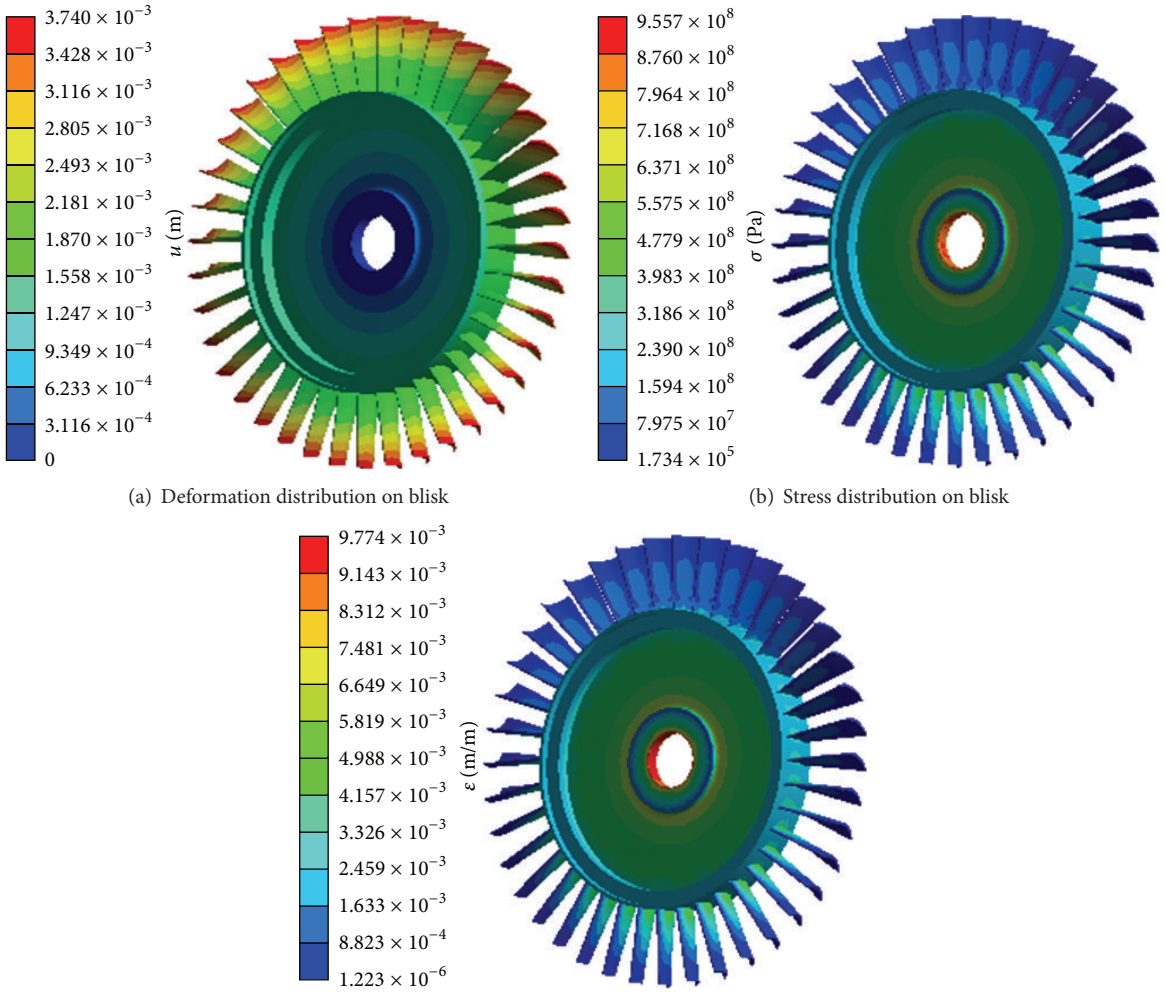

(a) Deformation distribution on blisk

(b) Stress distribution on blisk

(c) Strain distribution on blisk

Figure 7: Deformation, stress, and strain distribution on blisk.

and the thought of MRSM, the multiresponse surface model turbine blisk was established as follows:

$$\begin{aligned} y_1 &= -1.43 \times 10^{-2} + 9.8308 \times 10^{-5} v + 2.0023 \\ &\quad \times 10^{-9} p + 6.1827 \times 10^{-6} t + 1.1185 \times 10^{-6} \rho \\ &\quad + 1.6421 \times 10^{-6} w - 3.1758 \times 10^{-7} v^2 \\ &\quad - 1.6927 \times 10^{-15} p^2 - 2.6173 \times 10^{-9} t^2 \\ &\quad - 8.1784 \times 10^{-11} \rho^2 + 7.0349 \times 10^{-10} w^2, \\ y_2 &= 3.5147 \times 10^{8} - 8.179 \times 10^{6} v + 1.6905 \times 10^{3} p \\ &\quad + 1.7985 \times 10^{6} t + 9.3053 \times 10^{3} \rho - 1.3004 \\ &\quad \times 10^{6} w + 2.5955 \times 10^{4} v^2 - 1.386 \times 10^{-3} p^2 \\ &\quad - 19.2157 t^2 - 0.6358 \rho^2 + 6.1378 \times 10^{2} w^2, \end{aligned}$$

Table 2: Single-object sampling statistics of blisk.

Object variables	Maximum allowable values	Sampling number
y_1/m	$\leq 3.7 \times 10^{-3}$	9942
y_2/Pa	$\leq 1.07 \times 10^{9}$	9935
y_3/m/m	$\leq 1.12 \times 10^{-2}$	9954

$$\begin{aligned} y_3 &= 0.0045 - 8.7321 \times 10^{-5} v + 1.822 \times 10^{-8} p \\ &\quad + 1.6927 \times 10^{-5} t + 1.0621 \times 10^{-7} \rho + 1.3835 \\ &\quad \times 10^{-5} w + 2.7717 \times 10^{-7} v^2 - 1.494 \\ &\quad \times 10^{-14} p^2 + 9.7086 \times 10^{-10} t^2 - 7.515 \\ &\quad \times 10^{-12} \rho^2 + 6.5152 \times 10^{-9} w^2. \end{aligned} \tag{15}$$

When the maximum allowable deformation, stress, and strain of turbine blisk are $u_{a_1} = 3.7 \times 10^{-3}$ m, $\sigma_a = 1.07 \times 10^9$ Pa, and $\varepsilon_a = 1.12 \times 10^{-2}$ m/m, the built multiresponse surface model was simulated by 10 000 times using MCM. The analytical results are listed in Table 2. The histograms and

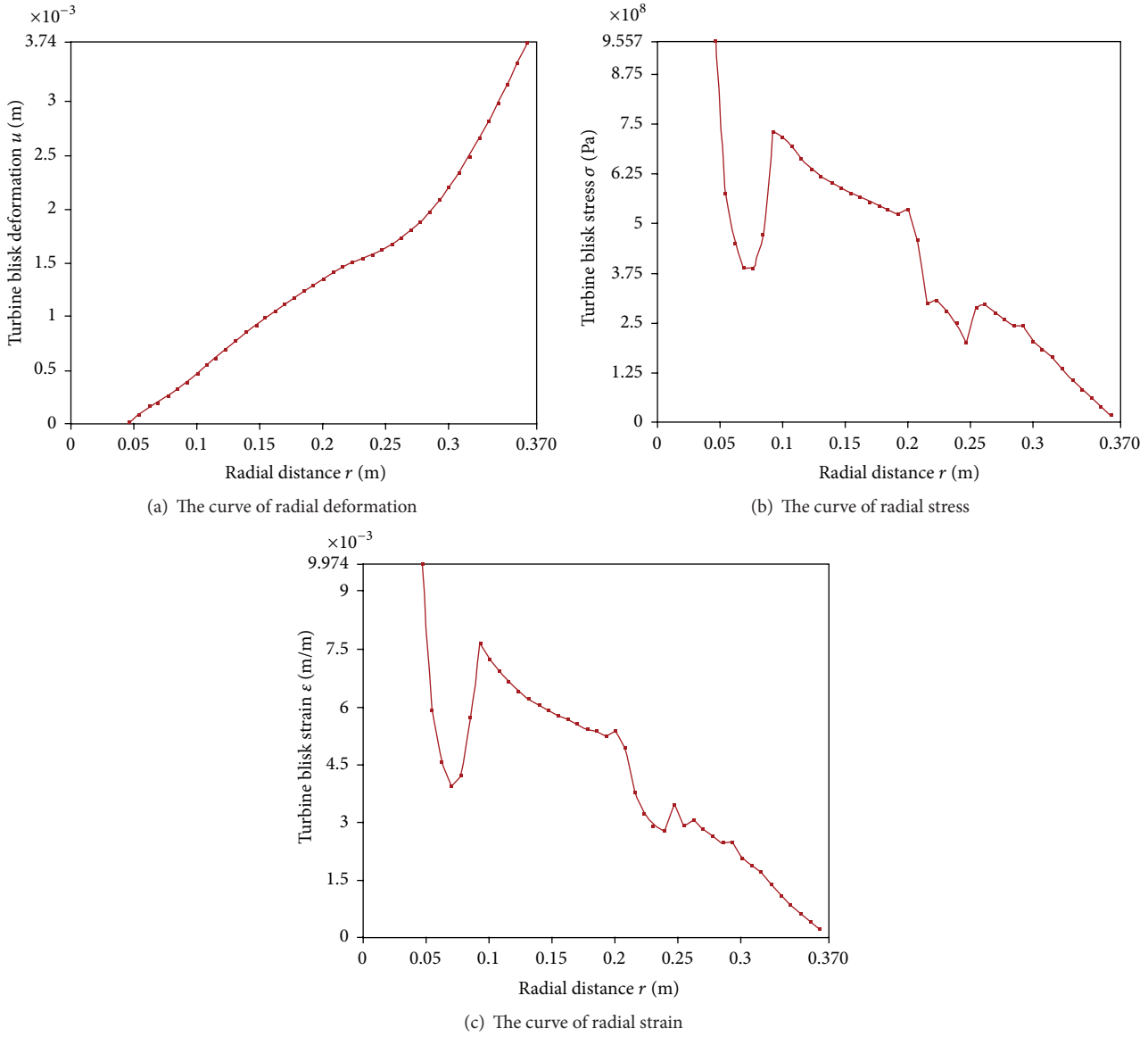

(a) The curve of radial deformation

(b) The curve of radial stress

(c) The curve of radial strain

FIGURE 8: The curves of turbine blisk deformation, stress, and strain along radial direction.

TABLE 3: Multiobject sampling statistics of blisk.

y_1/m, y_2/Pa, y_3/m/m	Number of samples
$y_1 \le 3.7 \times 10^{-3} \cap y_2 \le 1.07 \times 10^9 \cap y_3 \le 1.12 \times 10^{-2}$	9919
$y_1 > 3.7 \times 10^{-3} \mid y_2 > 1.07 \times 10^9 \mid y_3 > 1.12 \times 10^{-2}$	81

simulation history curves of maximum deformation u_{max}, maximum stress σ_{max}, and maximum strain ε_{max} are shown in Figures 9 and 10, respectively. Through the comprehensive performance evaluation, the results were summarized in Table 3.

As shown in Figure 10, the output responses (deformation y_1, stress y_2, and strain y_3) for turbine blisk obey normal distributions with the corresponding mean values of 3.452×10^{-3} m, 9.974×10^8 Pa, and 1.040×10^{-2} m/m and the corresponding standard deviation of 8.476×10^{-9} m, 7.672×10^2 Pa, and 8.385×10^{-8} m/m, respectively. From Table 2, it is illustrated that the reliability degrees for the deformation, stress, and strain of turbine blisk are 0.9942, 0.9935, and 0.9954, respectively. The above conclusions pledge the reliability and security of turbine blisk design.

As revealed in Table 3, the comprehensive reliability degree of turbine blisk is obtained as 0.9919 through joint reliability analysis, which basically meets the design requirement of aeroengine turbine blisk.

5. Conclusions

The goal of this effort is to apply the high accuracy and high efficiency MRSM to the comprehensive reliability evaluation

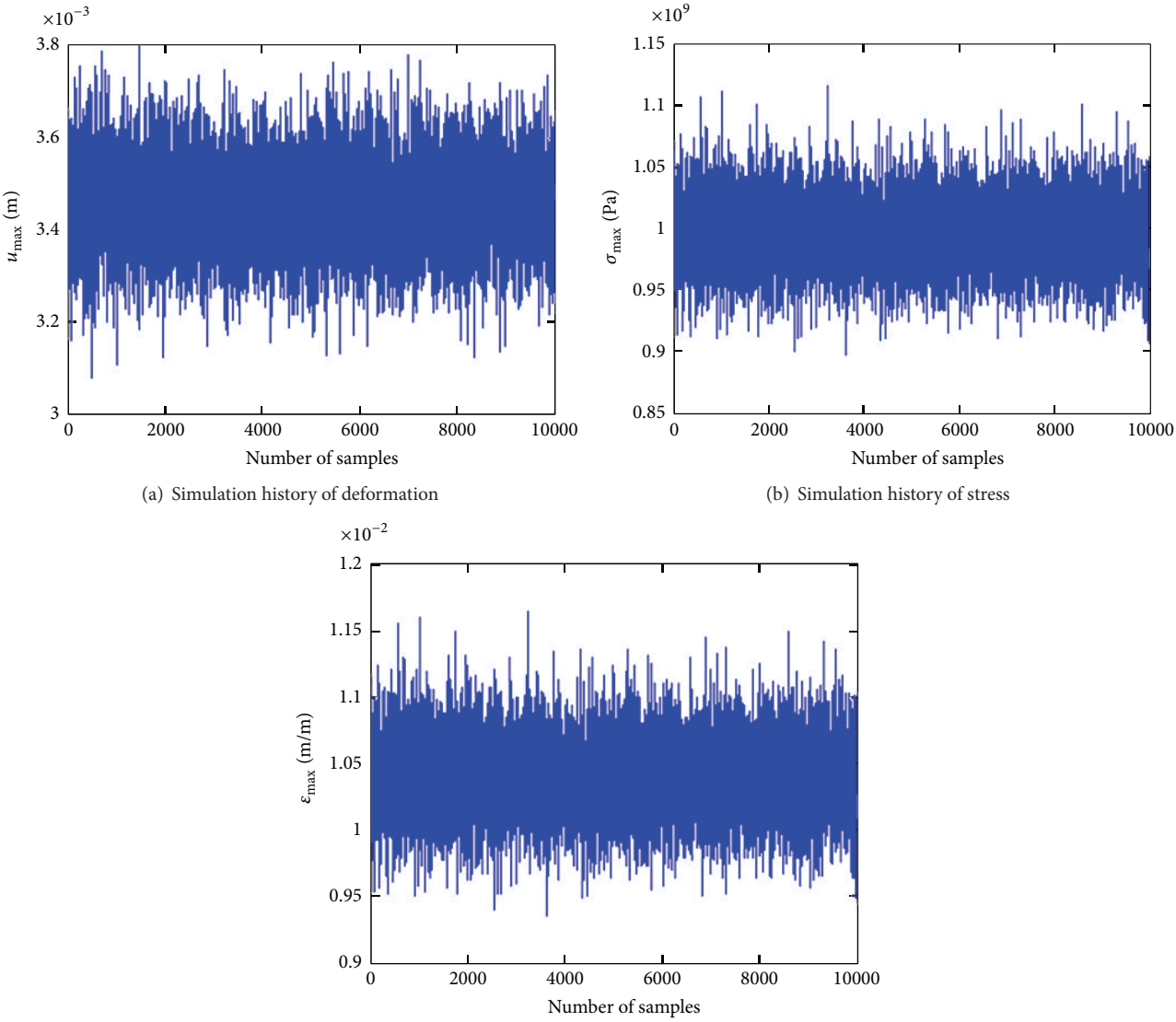

(a) Simulation history of deformation

(b) Simulation history of stress

(c) Simulation history of strain

Figure 9: Simulation samples of turbine blisk.

of aeroengine turbine blisk through the multiobject reliability analyses of the deformation, stress, and stress of turbine blisk based on fluid-thermal-structural coupling analysis. The present study establishes the mathematical model of MRSM with the quadratic response surface function. Some conclusions are drawn as follows:

(1) The maximum deformation, maximum stress, and maximum strain of blisk are 3.74×10^{-3} m, 9.557×10^{8} Pa, and 9.974×10^{-3} m/m, respectively. Besides, the distributions of blisk's deformation, stress, and strain are gained.

(2) The reliability degrees of blisk's deformation, stress, and strain are 0.9942, 0.9935, and 0.9954, respectively, when the allowable deformation, stress, and strain are $u_a = 3.7 \times 10^{-3}$ m, $\sigma_a = 1.07 \times 10^{9}$ Pa, and $\varepsilon_a = 1.12 \times 10^{-2}$ m/m, respectively. Based on the conclusions, the comprehensive reliability degree of blisk is 0.9919.

(3) The fluid-thermal-structural coupling analysis method is adopted for the reliability analysis of aeroengine turbine blisk, which is promising to improve computational accuracy.

(4) The efforts of this paper demonstrate that MRSM can be adopted to solve the comprehensive reliability analysis with multiple disciplines and multiple objects besides single-object reliability analysis, which provide a promising approach for complex structural reliability analysis.

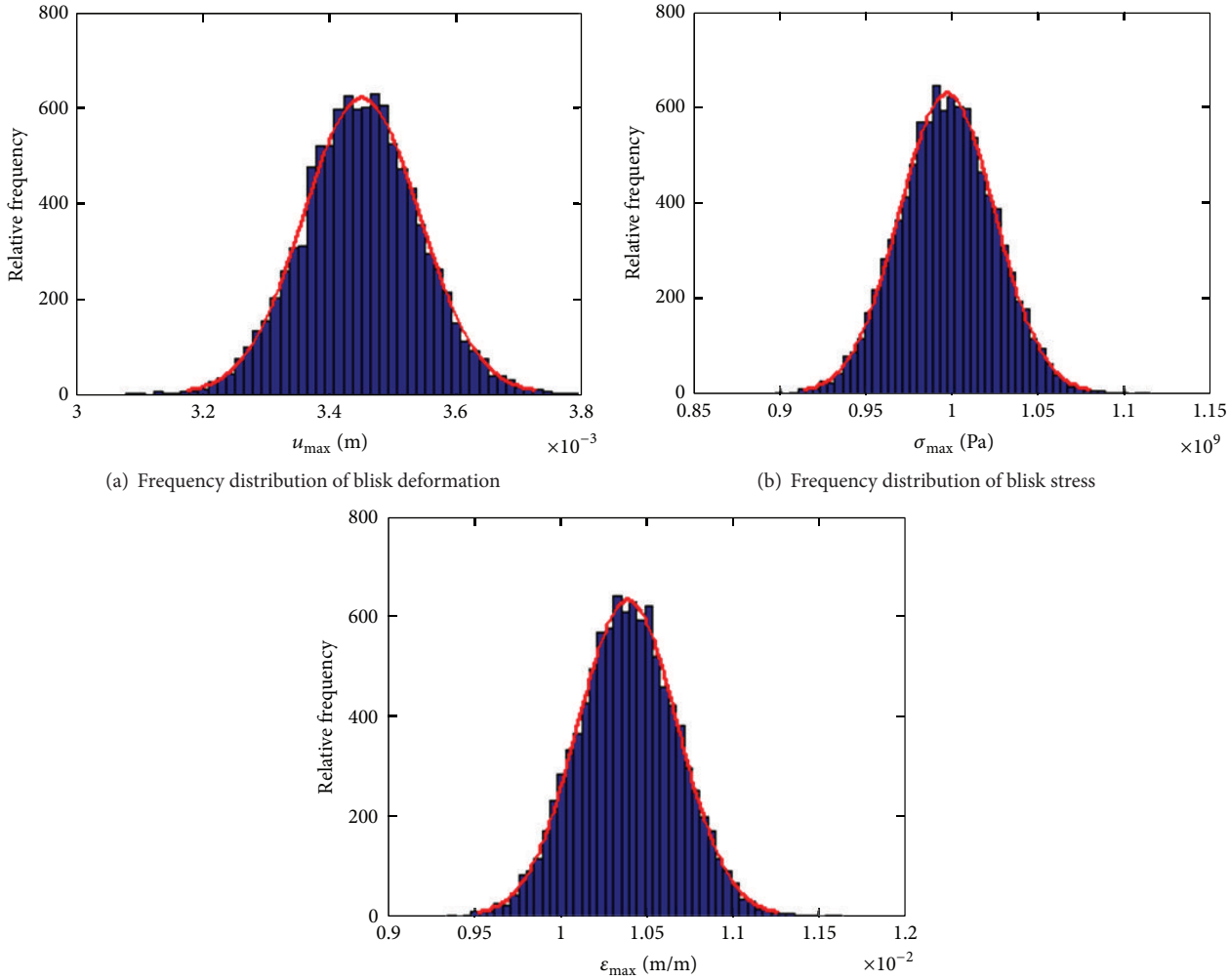

(a) Frequency distribution of blisk deformation

(b) Frequency distribution of blisk stress

(c) Frequency distribution of blisk strain

FIGURE 10: Frequency distribution of turbine blisk.

Conflict of Interests

The authors declare that there is no conflict of interests regarding the publication of this paper.

Acknowledgments

This paper is cosupported by the National Natural Science Foundation of China (Grants nos. 51275138 and 51475025), the Science Foundation of Heilongjiang Provincial Department of Education (Grant no. 12531109), and Hong Kong Scholars Program (Grant no. XJ2015002). The authors would like to thank them.

References

[1] S. B. Lattime and B. M. Steinetz, "High-pressure-turbine engine clearance control systems: current practices and future directions," *Journal of Propulsion and Power*, vol. 20, no. 2, pp. 302–311, 2004.

[2] S. B. Lattime, B. M. Steinetz, and M. G. Robbie, "Test rig for evaluating active turbine blade tip clearance control concepts," *Journal of Propulsion and Power*, vol. 21, no. 3, pp. 552–563, 2005.

[3] B. H. Jia and X. D. Zhang, "Study on effect of rotor vibration on tip clearance variation and fast active control of tip clearance," *Advanced Materials Research*, vol. 139–141, pp. 2469–2472, 2010.

[4] X.-M. Qi, Y. Piao, J.-H. Zhu, and J.-X. Zhou, "3-D numerical analysis of the tip clearance of an aero-engine high pressure turbine," *Journal of Aerospace Power*, vol. 23, no. 5, pp. 904–908, 2008.

[5] P. Pillidis and N. R. L. Maccallum, "Models for predicting tip clearance changes in gas turbines," NASA N83–229258, 1983.

[6] B. P. Wang, J. Wang, X. Z. Li, and Q. K. Han, "FE analysis on contact properties between root-blade and slot-disc," *Advanced Engineering Forum*, vol. 2-3, pp. 932–935, 2011.

[7] S. A. Meguid, R. H. Mao, and T. Y. Ng, "FE analysis of geometry effects of an artificial bird striking an aeroengine fan blade," *International Journal of Impact Engineering*, vol. 35, no. 6, pp. 487–498, 2008.

[8] Q. Lü and B. K. Low, "Probabilistic analysis of underground rock excavations using response surface method and SORM," *Computers and Geotechnics*, vol. 38, no. 8, pp. 1008–1021, 2011.

[9] M. E. Kartal, H. B. Başağa, and A. Bayraktar, "Probabilistic nonlinear analysis of CFR dams by MCS using response surface method," *Applied Mathematical Modelling*, vol. 35, no. 6, pp. 2752–2770, 2011.

[10] C. K. Fitzpatrick, M. A. Baldwin, P. J. Rullkoetter, and P. J. Laz, "Combined probabilistic and principal component analysis approach for multivariate sensitivity evaluation and application to implanted patellofemoral mechanics," *Journal of Biomechanics*, vol. 44, no. 1, pp. 13–21, 2011.

[11] A. Zona, M. Barbato, A. Dall'Asta, and L. Dezi, "Probabilistic analysis for design assessment of continuous steel-concrete composite girders," *Journal of Constructional Steel Research*, vol. 66, no. 7, pp. 897–905, 2010.

[12] D. Y. Hu, R. Q. Wang, and Z. Tao, "Probabilistic design for turbine disk at high temperature," *Aircraft Engineering and Aerospace Technology*, vol. 83, no. 4, pp. 199–207, 2011.

[13] T. Nakamura and K. Fujii, "Probabilistic transient thermal analysis of an atmospheric reentry vehicle structure," *Aerospace Science and Technology*, vol. 10, no. 4, pp. 346–354, 2006.

[14] C.-W. Fei, W.-Z. Tang, and G.-C. Bai, "Nonlinear dynamic probabilistic design of turbine disk-radial deformation using extremum response surface method-based support vector machine of regression," *Proceedings of the Institution of Mechanical Engineers G: Journal of Aerospace Engineering*, vol. 229, no. 2, pp. 290–300, 2015.

[15] C. W. Fei, G. C. Bai, and C. Tian, "Extremum response surface method for casing radial deformation probabilistic analysis," *Journal of Aerospace Information Systems*, vol. 10, no. 1, pp. 47–52, 2013.

[16] C. W. Fei and G. C. Bai, "Nonlinear dynamic probabilistic analysis for turbine casing radial deformation using extremum response surface method based on support vector machine," *Journal of Computational and Nonlinear Dynamics*, vol. 8, no. 4, Article ID 041004, 2013.

[17] C. W. Fei, G. C. Bai, and W. Z. Tang, "Probabilistic design of HPT blade-tip radial running clearance with distributed collaborative response surface method," *Journal of Aerospace Engineering*, vol. 28, no. 2, Article ID 04014069, 2015.

[18] X. Zhai, C.-W. Fei, Q.-G. Zhai, and J.-J. Wang, "Reliability and sensitivity analyses of HPT blade-tip radial running clearance using multiply response surface model," *Journal of Central South University*, vol. 21, no. 11, pp. 4368–4377, 2014.

[19] C.-W. Fei and G.-C. Bai, "Distributed collaborative probabilistic design for turbine blade-tip radial running clearance using support vector machine of regression," *Mechanical Systems and Signal Processing*, vol. 49, no. 1-2, pp. 196–208, 2014.

[20] Y. J. Song, G. L. Yu, L. M. Song, J. Li, and Z. P. Feng, "Multi-objective and multi-disciplinary design optimization of high temperature blade based on heat-fluid-solid coupling analysis," *Journal of Engineering Thermophysics*, vol. 35, no. 12, pp. 2367–2371, 2014.

[21] L. Li, Y.-S. Li, L.-B. Ao, and Z.-F. Yue, "Thermal-solid coupling analysis of centrifugal compressor," *Tuijin Jishu/Journal of Propulsion Technology*, vol. 30, no. 4, pp. 425–429, 2009.

[22] Y. C. Nho, J. S. Park, Y. J. Lee, and J. S. Kwak, "Effects of turbine blade tip shape on total pressure loss and secondary flow of a linear turbine cascade," *International Journal of Heat and Fluid Flow*, vol. 33, no. 1, pp. 92–100, 2012.

[23] C. E. Wang, "Integrated aerodynamic design and analysis of turbine blades," *Advances in Engineering Software*, vol. 68, no. 1, pp. 9–18, 2014.

[24] H. Farrokhfal and A. R. Pishevar, "Aerodynamic shape optimization of hovering rotor blades using a coupled free wake–CFD and adjoint method," *Aerospace Science and Technology*, vol. 28, no. 1, pp. 21–30, 2013.